Sarcomere length nanometry in rat neonatal cardiomyocytes expressed with α-actinin–AcGFP in Z discs

Seine A. Shintani,[1] Kotaro Oyama,[1] Fuyu Kobirumaki-Shimozawa,[2] Takashi Ohki,[1] Shin'ichi Ishiwata,[1,3] and Norio Fukuda[2]

[1]Department of Pure and Applied Physics, Faculty of Science and Engineering, Waseda University, Shinjuku-ku, Tokyo 169-8555, Japan
[2]Department of Cell Physiology, The Jikei University School of Medicine, Minato-ku, Tokyo 105-8461, Japan
[3]Waseda Bioscience Research Institute in Singapore, Helios, Singapore 138667

Nanometry is widely used in biological sciences to analyze the movement of molecules or molecular assemblies in cells and in vivo. In cardiac muscle, a change in sarcomere length (SL) by a mere ∼100 nm causes a substantial change in contractility, indicating the need for the simultaneous measurement of SL and intracellular Ca^{2+} concentration ($[Ca^{2+}]_i$) in cardiomyocytes at high spatial and temporal resolution. To accurately analyze the motion of individual sarcomeres with nanometer precision during excitation–contraction coupling, we applied nanometry techniques to primary-cultured rat neonatal cardiomyocytes. First, we developed an experimental system for simultaneous nanoscale analysis of single sarcomere dynamics and $[Ca^{2+}]_i$ changes via the expression of AcGFP in Z discs. We found that the averaging of the lengths of sarcomeres along the myocyte, a method generally used in today's myocardial research, caused marked underestimation of sarcomere lengthening speed because of the superpositioning of different timings for lengthening between sequentially connected sarcomeres. Then, we found that after treatment with ionomycin, neonatal myocytes exhibited spontaneous sarcomeric oscillations (cell-SPOCs) at partial activation with blockage of sarcoplasmic reticulum functions, and the waveform properties were indistinguishable from those obtained in electric field stimulation. The myosin activator omecamtiv mecarbil markedly enhanced Z-disc displacement during cell-SPOC. Finally, we interpreted the present experimental findings in the framework of our mathematical model of SPOCs. The present experimental system has a broad range of application possibilities for unveiling single sarcomere dynamics during excitation–contraction coupling in cardiomyocytes under various settings.

The Journal of General Physiology

INTRODUCTION

The state of the contractile system of cardiac muscle is regulated by a change in the intracellular Ca^{2+} concentration ($[Ca^{2+}]_i$), regardless of the development stage (Bers, 2002; Colella et al., 2008 and references therein). It is likewise well established that cardiac contractile performance is highly dependent on sarcomere length (SL) in that a change of merely ∼100 nm causes a substantial change in myocardial contractility (i.e., the Frank-Starling relation; Allen and Kentish, 1985; Fukuda et al., 2001; Katz, 2002; Hanft et al., 2008). This intrinsic nature of cardiac myofilaments requires an accurate measurement of SL to enhance our understanding of myocardial dynamic properties, not only in adults but also in neonates whose cardiomyocytes undergo rapid growth for normal heart development via biochemical/paracrine and mechanical signaling (Jacot et al., 2008, 2010; Rodriguez et al., 2011 and references therein). However, because of the lack of technology to measure single SL at high spatial and temporal resolution, sarcomere dynamics and the impact on myocyte motion have not been systematically investigated, especially in neonatal cardiomyocytes.

Although several studies have been conducted by using various types of cardiac specimens, either neonatal or adult, SL is usually averaged along myofibrils. However, given the notion that $[Ca^{2+}]_i$ rises locally in cardiomyocytes (in both adults [Bers, 2002] and neonates [Colella et al., 2008]), it is imperative to investigate how the mechanical properties of myocytes are fine-tuned via single sarcomere dynamics. Recently, we applied quantum dots (QDs) to isolated adult cardiomyocytes and successfully measured the length of a single sarcomere at 30-nm spatial precision at 30 fps (Serizawa et al., 2011). However, given the notion that only a small fraction of QDs were incorporated into living myocytes, even with the use of FuGene, the properties of sarcomeric motion in relation to a change in $[Ca^{2+}]_i$ could not be analyzed in detail (Serizawa et al., 2011).

Correspondence to Norio Fukuda: noriof@jikei.ac.jp; or Shin'ichi Ishiwata: ishiwata@waseda.jp

Abbreviations used in this paper: FI, fluorescence intensity; OM, omecamtiv mecarbil; QD, quantum dot; SHG, second harmonic generation; SL, sarcomere length; SPOC, spontaneous sarcomeric oscillation.

The Rockefeller University Press $30.00
J. Gen. Physiol. Vol. 143 No. 4 513–524
www.jgp.org/cgi/doi/10.1085/jgp.201311118

α-Actinin is a 100-kD filamentous actin–binding protein that is concentrated in the dense bodies of stress fibers and smooth muscle cells and in the Z discs of striated muscle cells. Dabiri et al. (1997) first demonstrated green fluorescent protein fusion to the amino terminus of α-actinin in living chick embryonic cardiomyocytes and provided evidence that muscle thick and thin filaments were assembled in different cellular locations to form the sarcomeric structure. Recently, by taking advantage of this method, Hersch et al. (2013) estimated the contractile force of rat neonatal cardiomyocytes.

In the present study, we coupled AcGFP to α-actinin and transfected rat neonatal cardiomyocytes to directly visualize single sarcomeric movements at nanometer precision simultaneously with $[Ca^{2+}]_i$. Results clearly show that (a) the coordinated movements of sarcomeres in series produce motion of a given region of a myocyte; (b) single sarcomeric oscillation waveforms during electric field stimulation are indistinguishable from the spontaneous sarcomeric oscillations (SPOCs) occurring at constant, partial $[Ca^{2+}]$ in skinned myocardium (termed cell-SPOC; Sasaki et al., 2006; Ishiwata et al., 2011; Serizawa et al., 2011); and (c) the myosin activator omecamtiv mecarbil (OM) enhances Z-disc movements during cell-SPOC. Moreover, the preset experimental system was useful for the measurement of SL displacement in adult ventricular myocytes. The molecular mechanisms of cardiac sarcomere dynamics under various conditions, as well as the application possibilities of our experimental system, are discussed.

MATERIALS AND METHODS

AcGFP expression in the Z discs of neonatal cardiomyocytes

All of the experiments in this study conformed to the Guide for the Care and Use of Laboratory Animals published by the National Institutes of Health (NIH publication No. 85-23, revised in 1996).

Ventricular myocytes were isolated from 1-d-old Wistar rats and were cultured based on a previous publication (Kojima et al., 2003). pAcGFP-actinin plasmid transfection was performed on the third day of incubation by using Lipofectamine LTX (Invitrogen). pAcGFP-actinin plasmids were obtained by inserting the α-actinin gene into pAcGFP-N1 (Takara Bio Inc.).

Microscopic system

Real-time nanoimaging was performed on AcGFP-expressing neonatal myocytes by using an inverted microscope (IX-70; Olympus) equipped with an electron-multiplying charge coupled device camera (iXon +897; Andor Technology) using a 60× oil immersion objective (numerical aperture of 1.45; Olympus; Oyama et al., 2012). Fluorescence images were obtained from myocytes expressed with α-actinin–AcGFP. When changes in $[Ca^{2+}]_i$ were measured simultaneously with sarcomeric motion, the myocytes were bathed in 2 mM Ca^{2+}-HEPES-Tyrode's solution containing 2 µM Fluo-4-AM (Dojindo) for 20 min at 25°C. Thereafter, experiments were performed.

As a general rule of optics, spatial precision decreases with an increase in camera speed (frame rate). Therefore, to obtain high precision in the measurement of SL displacement, we imaged sarcomeric motions at 50 fps in the majority of the experiments in this study (Drago et al., 2012).

Experimental procedure

Nanoscale imaging was performed 1 d after pAcGFP-actinin plasmid transfection. In experiments under electric field stimulation, 2 mM Ca^{2+}-HEPES-Tyrode's solution was used as the bathing solution, and myocytes were electrically stimulated (Serizawa et al., 2011 and references therein). For experiments on cell-SPOC, myocytes were treated with 4 µM ionomycin (Sigma-Aldrich) to increase the Ca^{2+} permeability of the membranes. Then, they were bathed in Ca-SPOC solution (pCa 5.75 buffered by Ca^{2+}/10 mM EGTA; see the Methods section of the online supplemental material) containing 4 µM thapsigargin (Sigma-Aldrich) and 200 µM ryanodine (Sigma-Aldrich). OM (Selleck) was initially dissolved in ethanol and diluted with 0.6 µM Ca-SPOC solution. The final concentration of ethanol was 0.1%, having no effect on cell-SPOC.

Except for the experiment on spontaneous beating (performed at 27 ± 0.5°C), all the mechanical experiments were performed at 36.0 ± 0.5°C in this study. When changes in $[Ca^{2+}]_i$ were measured simultaneously with sarcomeric motion, the myocytes were bathed in the 2 mM Ca^{2+}-HEPES-Tyrode's solution containing 2 µM Fluo-4-AM for 20 min at 25 ± 0.5°C. Thereafter, the imaging experiments were performed at 36.0 ± 0.5°C.

Data analysis

The intensity profiles of the fluorescence images were obtained by iQ software (Andor Technology), transferred to ImageJ software (National Institutes of Health), and analyzed by using our Microsoft Excel macro, as described in previous studies (Sasaki et al., 2006; Serizawa et al., 2011). In both the electric field stimulation and cell-SPOC experiments, we obtained the following parameters as indices of sarcomeric contraction: SL oscillation frequency, SL amplitude, sarcomere shortening time (velocity), sarcomere lengthening time (velocity), and Z-disc amplitude. The SL amplitude was defined as the SL at peak lengthening minus that at peak shortening. The shortening (lengthening) time was defined as the length of time from the onset to the end of SL shortening (lengthening). The Z-disc amplitude was defined as the distance of the movement of the Z disc during a cycle of contraction. Data obtained from three consecutive contraction cycles were averaged for the aforementioned parameters.

Statistics

Significant differences were assigned using the paired or unpaired *t* test as appropriate. Data are expressed as means ± SEM unless otherwise noted, with *n* representing the number of preparations. Linear regression analyses were performed in accordance with the method used in a previous study (Fukuda et al., 2001). Statistical significance was assumed to be $P < 0.05$. NS indicates $P > 0.05$.

Online supplemental material

Supplemental text provides more information about the methods used in this paper. Fig. S1 presents image analysis for a rat neonatal cardiomyocyte transfected with the α-actinin–AcGFP plasmid showing the colocalization of α-actinin–AcGFP with the phase-dense Z discs. Fig. S2 shows the fluctuation analysis of the length of a single sarcomere in an α-actinin–AcGFP-expressing neonatal cardiomyocyte in the presence of Fluo-4. Fig. S3 shows changes in SL and fluorescence intensity (FI) in a cardiomyocyte upon electric stimulation in the absence of Fluo-4. Fig. S4 shows α-actinin–AcGFP expression and SL nanometry in an adult cardiomyocyte of the rat. Fig. S5 shows the time course of changes in the lengths of sarcomeres during spontaneous beating in an AcGFP-expressing neonatal cardiomyocyte. Fig. S6 presents histograms showing averaged data versus individual data on amplitude, shortening,

and lengthening properties during spontaneous beating. Fig. S7 shows sarcomeric motions during spontaneous beating in a neonatal cardiomyocyte without transfection of the α-actinin–AcGFP plasmid. Fig. S8 shows the relationship of electric stimulation frequency versus time to peak FI in intact neonatal cardiomyocytes. Fig. S9 shows cell-SPOC properties in AcGFP-expressing neonatal cardiomyocytes. Fig. S10 shows waveform analyses of cell-SPOC in the absence and presence of OM. Videos 1 and 2 show neonatal cardiomyocytes expressed with α-actinin–AcGFP in Z discs at rest. Video 3 shows reconstruction of a three-dimensional image of a neonatal cardiomyocyte. Video 4 shows that the FI from a near full range of a cardiomyocyte does not change during the course of sarcomeric contraction. Video 5 shows an adult cardiomyocyte expressed with α-actinin–AcGFP in Z discs at rest. Videos 6 and 7 present neonatal cardiomyocytes showing spontaneous beating. Videos 8 and 9 present neonatal cardiomyocytes showing contractions in response to electric field stimulation. Videos 10–12 present neonatal cardiomyocytes showing cell-SPOC. Online supplemental material is available at http://www.jgp.org/cgi/content/full/jgp.201311118/DC1.

RESULTS AND DISCUSSION

First, the α-actinin–AcGFP construct produced fluorescent-labeled protein in Z discs within 24 h after transfection when introduced into neonatal myocytes (as demonstrated in neonatal chick [Dabiri et al., 1997] and rat myocytes [Hersch et al., 2013]; Fig. 1 A). This fusion protein was incorporated into the Z discs of normal cellular structures rich in endogenous α-actinin, and α-actinin–AcGFP colocalized in a banded pattern with the phase-dense Z discs (Fig. S1).

As shown in the plot profile in Fig. 1 A, SL averaged ∼1.95 µm under the resting condition (1.965 ± 0.021 µm; from 10 myocytes × 3 sarcomeres). This value is similar to that reported previously in rat neonatal myocytes (Hersch et al., 2013), and it is slightly longer than that reported by others in isolated adult rat and mouse myocytes (i.e., ∼1.70–1.85 µm; Bub et al., 2010; King et al., 2011 and references therein; compare with Fig. S4). The differential value of SL is likely to primarily underlie the different experimental settings. Namely, in the present study, neonatal cardiomyocytes were cultured, as opposed to adult cardiomyocytes isolated from the heart in these previous studies. Also, it is likely that the differential titin (connectin) expression profile in neonatal versus adult cardiomyocytes may in part underlie the differential SL values. Indeed, Lahmers et al. (2004) reported that the titin expression profile in rats differs in adults versus neonates, with stiff N2B titin predominantly expressed in adults in contrast to more compliant neonatal isoforms (e.g., N2BA isoforms) expressed in neonates, with titin-based passive force ∼0 mN/mm^2 at SLs up to ∼2.0 µm. Given the widely accepted role of titin as a molecular ruler to determine the SL during myofibrillogenesis in striated muscles (Gregorio et al., 1999; Udaka et al., 2008 and references therein), the slightly longer SL observed in the present study under the isometric condition may be partly caused by N2BA titin isoforms predominantly expressed in neonatal myocytes.

The transfection efficacy of AcGFP expression in Z discs (i.e., the ratio of AcGFP-expressing myocytes [determined by fluorescence observation] to all myocytes attached to the glass plate [determined by phase-contrast observation]) was 38.14 ± 5.47% (number of observations, 17, at the image size of 138 × 138 µm with a 60× oil immersion objective).

Nanometry is a powerful technique that is widely used in single-molecule biophysics by many researchers for things like actomyosin interaction (Uemura et al., 2004; Komori et al., 2009; Kaya and Higuchi, 2010) and was recently used in molecular imaging in cells (Yoo et al., 2008; Watanabe et al., 2013) and even in vivo (Tada et al., 2007; Gonda et al., 2010) in various bioscience fields. In the present study, AcGFP was clearly expressed in Z discs in neonatal cardiomyocytes with relative ease via lipofection, providing a suitable experimental system for nanometry on a single SL displacement measurement (Fig. 1 B). Under the present experimental condition, the SL displacement precision was 3 nm at 50 fps (Fig. 1 B and Video 1). Likewise, it was 8 nm at 50 fps in the presence of the Ca^{2+} indicator Fluo-4 (Fig. S2 and Video 2). The present method (i.e., SL nanometry) provides high accuracy of the positioning of the AcGFP-expressed Z disc by fitting the 3 pixels, including the peak point (with the width of 0.81 µm), thereby minimizing the influence of the fluorescence of the neighboring Z discs (Fig. 1 B). Given a relatively short range of SL in cardiac preparations compared with that in skeletal muscle preparations, it can be considered that the present analysis provides a powerful tool in quantitating the SL displacement in cardiac muscle.

By moving the stage of the microscope (i.e., at 0.496 µm/s) in the Z direction (Video 3), the thickness of the myocyte in Fig. 1 A was estimated as ∼6 µm. However, considering the bleed over of the AcGFP fluorescence signal, this will be an overestimated value. To accurately measure the thickness of the myocyte cultured under the present setting, it will be necessary to measure the distance between the fluorescence beads (or nanoparticles) with a known diameter adhered to the top and bottom of the myocyte.

It is worth noting that because of the similar wavelengths of AcGFP (peak: 505 nm) and Fluo-4 (peak: 518 nm), the present experimental system enables simultaneous imaging of the SL displacement and $[Ca^{2+}]_i$ changes without the use of double light-path microscopy. As shown in Fig. S3 (also see Video 4), the FI obtained from the near full range of a cardiomyocyte did not change during the course of sarcomeric contraction (from ∼2.0 to ∼1.8 µm) in the absence of Fluo-4 during spontaneous beating, indicating that there was no interference of AcGFP and Fluo-4 fluorescence.

Clear striation patterns were likewise observed under confocal microscopy in isolated adult cardiomyocytes of the rat by using the adenovirus vector system, enabling

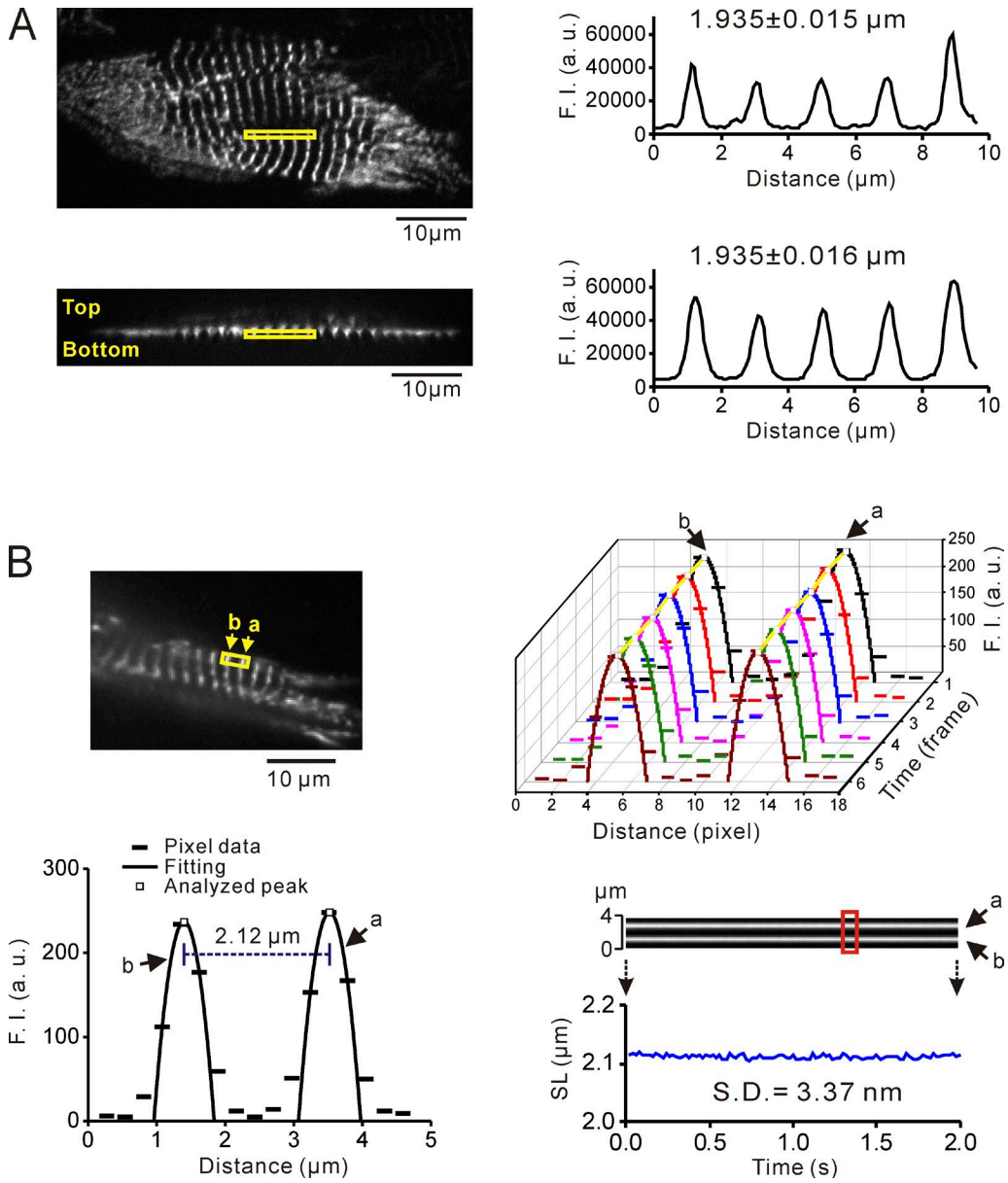

Figure 1. SL nanometry in α-actinin–AcGFP-expressing rat neonatal cardiomyocytes. (A, top left) Epi-illumination image of a neonatal cardiomyocyte expressed with α-actinin–AcGFP. (left, bottom) Side view of the reconstructed image of the myocyte at the top left. "Top" or "bottom" indicates the direction (i.e., "bottom" attached to the cover glass). See Video 3. (top right) Plot profile of the yellow outlined rectangular region in the image at the top left. (bottom right) Plot profile of the yellow outlined rectangular region in the image at the bottom left. Numbers in plot profiles indicate the values of mean lengths of seven sarcomeres viewed from different angles (NS, $P > 0.05$ compared with the value at the top right). (B, top left) Epi-illumination image of a neonatal cardiomyocyte expressed with α-actinin–AcGFP in Z discs. Imaging performed at rest; clip from Video 1. The sarcomere in the yellow outlined rectangle was used for the analysis. (bottom left) A graph showing an example of SL nanometry. Fluorescence peak was fitted by a parabolic function of $Y = -AX^2 + BX - C$ (A, B, and C are constants) using 3 pixels (i.e., peak and before and after the peak) at each camera frame to obtain the midpoint for the curve. a: A, B, and C, 1,227.7, 3,435.2, and 2,166.0, respectively ($X = 3.521$ μm). b: A, B, and C, 1,207.1, 8,500.0, and 1,4715.0, respectively ($X = 1.399$ μm). 1 pixel, 270 nm (for all experiments with neonatal cardiomyocytes). Because of the mathematical nature, the parabolic function passes all 3 pixels. The midpoint of the parabolic function was defined as the Z-disc position, and SL was derived by the difference between the adjacent two midpoint values. (top right) A three-dimensional graph showing changes in the positions of a and b from frame 1 (same as in bottom left) to 6. Yellow lines, time-dependent changes in the Z disc. (middle right) Kymographs showing changes in the longitudinal positions of the AcGFP fluorescence signals. a and b indicate the AcGFP fluorescence signals in the yellow outlined rectangle in the top left image. Time course, 2 s (as shown by dashed arrows). The time period shown by a red rectangle was used for the analysis in the top right. (bottom right) Fluctuation of the length of a single sarcomere (distance between a and b). SD (i.e., SL displacement precision) was 3.37 nm. a.u., arbitrary units.

us to measure single SL displacement with 15-nm precision at 30 fps (Fig. S4 and Video 5). It should be noted that this value is approximately twofold greater than that obtained in our previous study using QDs conjugated with anti–α-actinin antibody (i.e., 30-nm precision at 30 fps; Serizawa et al., 2011), indicating the usefulness of our experimental system in the analysis of sarcomere dynamics in isolated adult cardiomyocytes. In the present study, however, we systematically investigated the single sarcomere dynamics in cultured neonatal cardiomyocytes, taking into consideration the following three merits. First, experiments can be performed under the isometric condition (hence the results can be simply extrapolated to the previous findings obtained from skinned fibers/myocytes of various cardiac specimens). Second, a very high precision (∼3 nm) in the measurement of SL displacement can be obtained with no need for a confocal system because of a thin layer of myofibrils (compare with Fig. 1 A). Third, AcGFP can be routinely expressed with a success rate of ∼40% in Z discs via lipofection (i.e., no need for advanced gene expression techniques). Future research will need to thoroughly investigate the sarcomere dynamics in both healthy and diseased adult cardiomyocytes at nanometer precision.

It is well known that spontaneous, periodic releases of Ca^{2+} occur from the SR in cultured neonatal myocytes under physiological conditions, subsequently inducing contractions with large sarcomeric amplitudes (Jacot et al., 2008, 2010; Rodriguez et al., 2011; Hersch et al., 2013). Because the advantage of the present method is to track the individual SL instead of measuring the mean value, we conducted simultaneous imaging of single sarcomeres and $[Ca^{2+}]_i$ in α-actinin–AcGFP-expressing myocytes during spontaneous beating (at ∼1 Hz; see Fig. 2 A for six consecutive beats; also see Video 6). The striations of AcGFP fluorescence were clearly seen along the myocyte even after the loading of the Ca^{2+} indicator Fluo-4 during the course of beating, with Fluo-4 fluorescence increasing only in the SL shortening phase. We then conducted in-depth SL analyses on the second and third beats (Fig. 2 B). It was found that sarcomeres first shortened by ∼0.3 µm in response to a rise in $[Ca^{2+}]_i$ (phase 1), followed by quick lengthening (phase 2) and subsequent shortening to the original SL (phase 3). Although phase 1 was observed in all sarcomeres within the myocyte, phase 2 (and the subsequent phase 3) was observed in a time-dependent and SL-dependent manner (Fig. S5), independent of $[Ca^{2+}]_i$ (see Fig. 2 B, top, a kymograph, for similar $[Ca^{2+}]_i$ changes in various sarcomeres). Namely, sarcomeres with lengths longer than the mean value (∼1.95 µm in this myocyte) were lengthened in a consecutive manner, and shorter sarcomeres did not exhibit the lengthening phase, coupled presumably with a decrease in load on myofibrils. Our analysis revealed that the averaging of SL measurement caused marked underestimation of the lengthening speed as a result of delineation of the timing for lengthening between sequentially connecting sarcomeres (which occurred in a time-dependent and length-dependent manner). The histograms in Fig. S6 show that mean values differ from the individual values on shortening and lengthening properties and amplitude.

Here, it may be suggested that some sarcomeres are overstretched under the present experimental setting (i.e., up to ∼2.8 µm; Fig. 2, A and B). However, Opitz et al. (2004) demonstrated in rats that N2BA titin-expressing fetal/neonatal myofibrils produce passive force ∼15 times lower than that of adult myofibrils, and fetal/neonatal myofibrils can be reversibly elongated up to 3.5–4.0 µm (compare with 2.5–3.0 µm in N2B titin-expressing adult myofibrils). It is therefore likely that depending on the condition, sarcomeres can be elongated up to ∼2.8 µm in cultured neonatal cardiomyocytes of the rat, as observed in the present study. Future research will clarify the molecular mechanism of the propagation of lengthening/shortening of sarcomeres along myofibrils during spontaneous beating.

As evident by the finding of nonuniform sarcomere motion even within the same cell, it is reasonable to consider that our SL nanometry has broad potential to reveal slight but fundamental changes in sarcomere dynamics in neonatal as well as adult (Fig. S4) cardiomyocytes under various conditions. We consider that SL nanometry will enable nanoscale measurements of the displacement of the distance between dye-labeled T tubules in the isolated heart, not only when the heart is at rest (Bub et al., 2010; Serizawa et al., 2011; Botcherby et al., 2013; Inoue et al., 2013) but also in motion (e.g., in the beating heart in vivo).

The magnitude of SL shortening during spontaneous beating in myocytes with no AcGFP expression was similar to that observed in AcGFP-expressing myocytes (i.e., ∼0.3 µm; Fig. S7 and Video 7). This demonstrates that AcGFP expression in Z discs does not hinder sarcomeric contractile properties.

Recently, Llewellyn et al. (2008) successfully imaged sarcomere motion with the second harmonic generation (SHG) method. SHG allows for label-free imaging of the A band of the sarcomere at a subsarcomere precision and thus appears to be versatile for the investigation of sarcomere dynamics in various muscle types. However, the present method using the α-actinin–AcGFP expression provides (a) higher precision in the analysis of SL displacement (3 and 15 nm in neonatal and adult cardiomyocytes, respectively, as compared with 20–50 nm by using SHG; Boulesteix et al., 2004; Llewellyn et al., 2008); (b) nanoscale analysis of individual sarcomere dynamics without the use of smoothing techniques (which are frequently used in SHG; Llewellyn et al., 2008); (c) sharper fluorescence images based on the smaller width of Z discs than that of the A band; and (d) steady

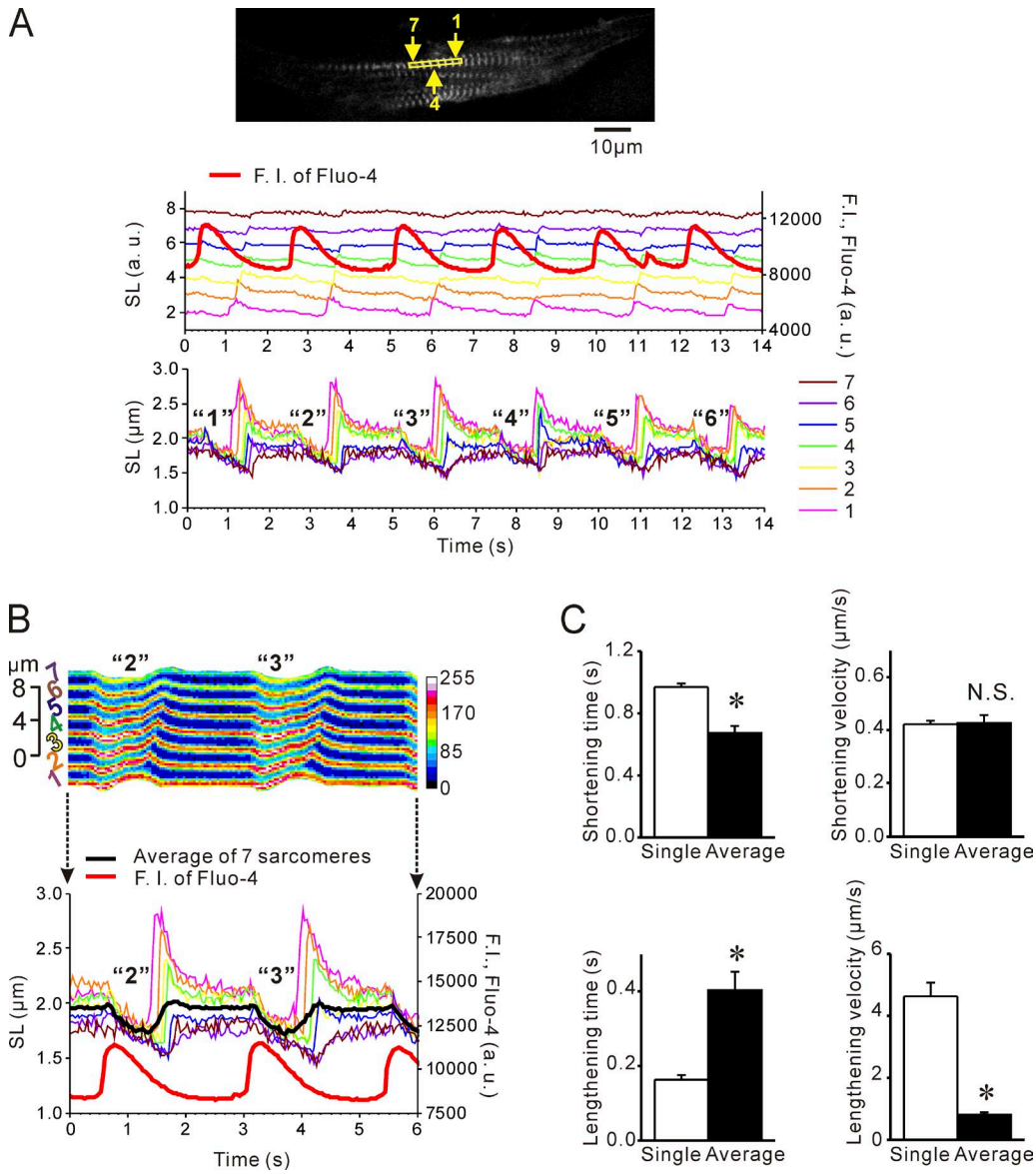

Figure 2. Simultaneous measurement of single SL and $[Ca^{2+}]_i$ in neonatal myocytes during spontaneous beating. (A, top) Epi-illumination image of an α-actinin–AcGFP-expressing myocyte loaded with Fluo-4. Numbers shown by arrows indicate sarcomeres used for the analyses. (middle) Time course of changes in the lengths of seven sarcomeres and the FI of Fluo-4. (bottom) Superimposed data showing SL changes. Six consecutive beats are shown. See Video 6. (B, top) Kymograph showing changes in the lengths of the seven sarcomeres (second and third beats; compare with A). Color bar at right indicates the pseudo-color representation of FI (arbitrary). (bottom) Graph showing changes in the lengths of the seven sarcomeres and the FI of Fluo-4 (second and third beats). Individual SL data (corresponding to the sarcomeres numbered with different colors in A), averaged SL data (black line), and $[Ca^{2+}]_i$ changes (red line) are shown on the same time course. (C, top) Bar graphs comparing the values of shortening time (left) and shortening velocity (right) obtained by using different types of analysis. (bottom) Bar graphs comparing the values of lengthening time (left) and lengthening velocity (right) by using different types of analysis. Single SL (averaged individual SL, from 1 to 7, during six consecutive beatings) versus averaged SL (from 1 to 7 during six consecutive beatings). *, $P < 0.05$. Error bars indicate means ± SEM. a.u., arbitrary units.

fluorescence images independent of the viewing angle (as compared with SHG; Plotnikov et al., 2006). In addition, our system allows for the simultaneous visualization of individual sarcomere dynamics and $[Ca^{2+}]_i$ changes at one wavelength excitation (with the precision of SL displacement of 8 nm in the presence of the Ca^{2+}-sensitive dye Fluo-4). Therefore, we consider that the present method using α-actinin–AcGFP expression is a more suitable choice than SHG for the analysis of excitation–contraction coupling in living cardiomyocytes at the individual sarcomere level.

Next, to investigate whether SL nanometry is indeed useful in analyzing sarcomere dynamics under conditions with electric field stimulation, i.e., an experimentation method frequently conducted in cardiac physiology, we simultaneously recorded the motion of single sarcomeres

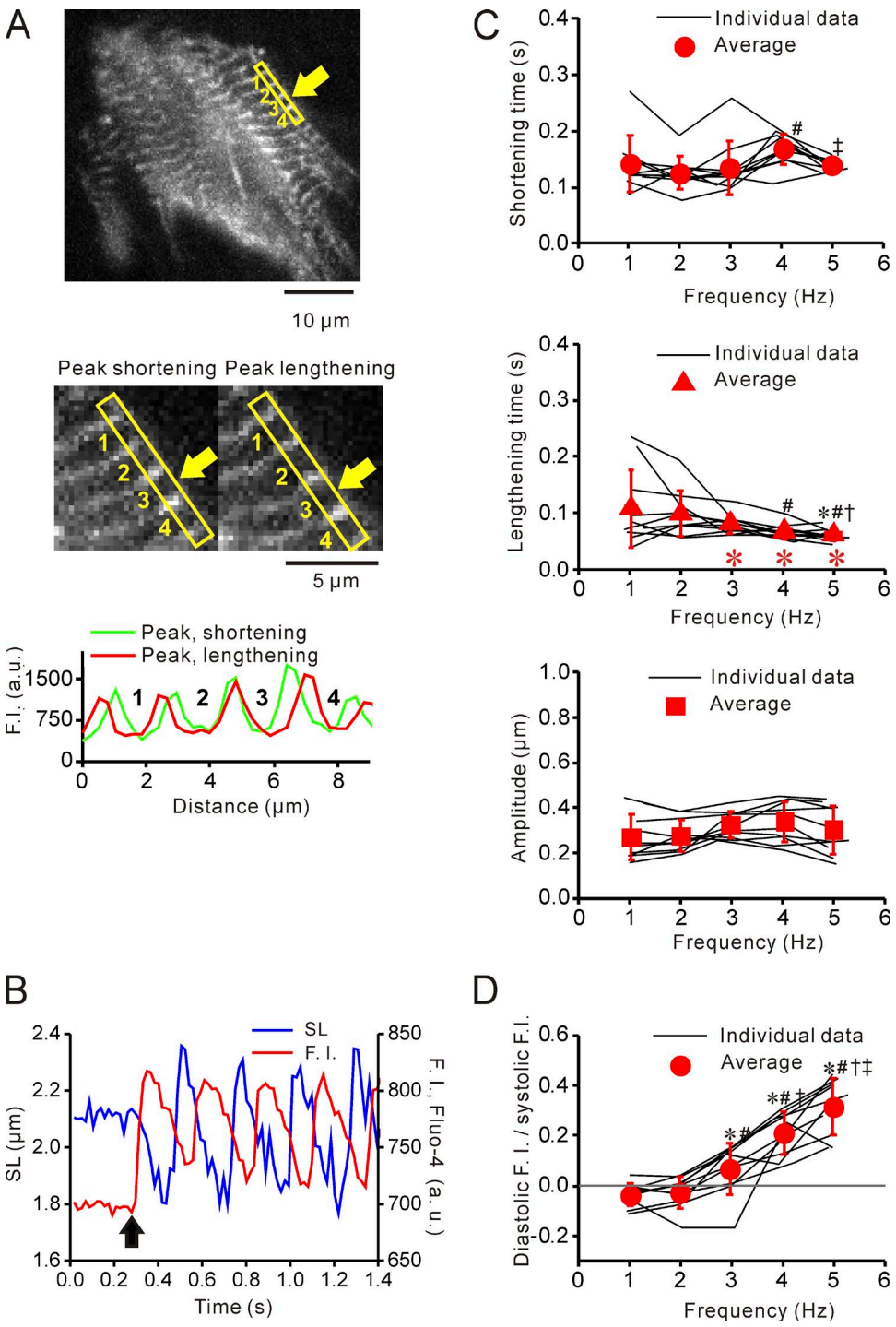

Figure 3. Simultaneous measurement of single SL and $[Ca^{2+}]_i$ in neonatal myocytes under electric field stimulation. (A, top) Epi-illumination image of an AcGFP-expressing myocyte loaded with Fluo-4 (image taken at rest); clip from Videos 8 and 9. Sarcomeres in the yellow outlined rectangle with numbers from 1 to 4 were used for the analysis. (middle) Enlarged view of the region of interest in the top image at peak shortening and peak lengthening with 1-Hz stimulation. (bottom) Plot profiles of the four sarcomeres at peak shortening and peak lengthening. Sarcomere numbers are indicated. (B) Time-dependent changes in SL and Fluo-4–dependent FI in an AcGFP-expressing neonatal cardiomyocyte. Sarcomere 3 in A was used for the analysis. The arrow indicates the onset of stimulation. (C) Relationship of stimulation frequency versus shortening time (top), lengthening time (middle), and SL amplitude (bottom). Data obtained at 1–5 Hz are summarized. Asterisks in red in the middle graph indicate a significant difference ($P < 0.05$) compared with the corresponding value in the top graph. (D) Relationship of stimulation frequency versus diastolic FI/systolic FI. Gray line, diastolic FI/systolic FI = 0. (C and D) *, $P < 0.05$; #, $P < 0.05$; †, $P < 0.05$; and ‡, $P < 0.05$ compared with the corresponding values at 1, 2, 3, and 4 Hz, respectively. Data taken from 10 myocytes, with one plot obtained from sequentially connecting three sarcomeres. Error bars indicate means ± SEM. a.u., arbitrary units.

and changes in $[Ca^{2+}]_i$ at various frequencies. Fig. 3 A shows a typical Fluo-4–loaded AcGFP-expressed myocyte at rest and at peak shortening and peak lengthening. Clear striation patterns at both phases indicate that our SL measurement system is of high precision regardless of the level of $[Ca^{2+}]_i$. Fig. 3 B represents typical recordings showing changes in SL and Fluo-4–dependent FI at 4 Hz (Video 8; also see Video 9 for stimulation at 2 Hz in the same myocyte). All the sarcomeres started to shorten (lengthen) almost simultaneously in response to a rise (decrease) in FI. By analyzing the waveform properties of single sarcomeres as a function of stimulation frequency, we found that the lengthening time decreased with little change in shortening time, resulting in a significant difference between shortening time and lengthening time at 3, 4, and 5 Hz (shortening time > lengthening time; $P < 0.05$; Fig. 3 C). However, the amplitude was unaffected by a change in stimulation frequency, which is consistent with the finding in a previous study with rat adult cardiomyocytes placed under the

isometric condition by using carbon fibers (Peterson et al., 2013).

Time to peak FI significantly decreased as frequency increased (Fig. S8), as previously demonstrated in adult mouse cardiomyocytes (Werdich et al., 2008). It is likewise important to note that diastolic FI significantly increased in a frequency-dependent manner ($P < 0.05$ at 3 Hz and higher; Fig. 3 D; Serizawa et al., 2011), despite the fact that these experiments were conducted at 36 ± 0.5°C. Thus, given high heartbeat frequencies in neonatal rats (∼240 bpm on day 0 and ∼300 bpm on day 1; Smotherman et al., 1991), it is considered that diastolic $[Ca^{2+}]_i$ is elevated in physiological settings, presumably as a result of insufficient SR Ca^{2+} pump activities (Serizawa et al., 2011 and references therein).

We previously reported that by using QD-treated isolated adult cardiomyocytes, a sarcomeric contraction cycle consisted of shortening followed by slow lengthening at a low frequency of 1 Hz, and a phase shift occurred upon an increase in stimulation frequency, in that the cycle consisted of shortening followed by quick lengthening at physiologically high frequencies (Serizawa et al., 2011). However, in the present study, shortening time was longer over the range of frequencies tested (Fig. 3 C). We consider that the difference in the waveform at a low frequency in the previous study (Serizawa et al., 2011) and the present study results primarily from the difference in the experimental condition (isotonic vs. isometric), rather than from the difference in the preparation (adult vs. neonatal).

Then, to further investigate the capability of SL nanometry under conditions in which the highest spatial resolution is obtained (i.e., with no interference of $[Ca^{2+}]_i$ changes), we analyzed sarcomeric waveform properties during SPOCs in ionomycin (Kauffman et al., 1980; Morgan and Jacob, 1994)-treated neonatal cardiomyocytes with SR functions blocked by ryanodine (Sutko et al., 1997) and thapsigargin (Davidson and Varhol, 1995; Treiman et al., 1998). Fig. 4 A shows an epi-illumination image of an α-actinin–AcGFP-expressing cardiomyocyte (left) and the waveforms of SPOC at two different time phases (right; Video 10; also see Video 11 for cell-SPOC with a low frequency of ∼1 Hz). Despite different magnitudes of Z-disc movement (at time phases 1 and 2), the amplitude of sarcomeric oscillation was similar (Fig. 4 A). As previously reported in studies on adult cardiac muscles of various animals (Sasaki et al., 2006; Ishiwata et al., 2011; Serizawa et al., 2011), cell-SPOC waves consisted of slow shortening followed by quick lengthening. In contrast to the situation in skinned adult cardiomyocytes in which the SPOC frequencies are relatively constant (and varies according to animal species; Sasaki et al., 2006; Ishiwata et al., 2011; Serizawa et al., 2011), relatively large cell-to-cell variations were observed (i.e., from ∼1 to ∼4.5 Hz; 2.08 ± 0.11 Hz on average from 31 myocytes) in ionomycin-treated neonatal myocytes, with the amplitude inversely correlated with frequency (Fig. 4 B). Likewise, the shortening time/lengthening time ratio decreased with an increase in frequency (Fig. 4 C) as a result of a frequency-dependent decrease in shortening time with no significant change in lengthening time (Fig. S9). It should be stressed that at a physiologically relevant frequency of 4 Hz, the values in the relationships in Fig. 4 (B and C) became statistically indistinguishable between electric field stimulation and cell-SPOC, suggesting that the sawtooth waveform is intrinsic to sarcomeres themselves, with and without changes in $[Ca^{2+}]$ (Sasaki et al., 2006; Ishiwata et al., 2011). When converted to velocity, it was found that shortening velocity increased and lengthening velocity decreased, both in a linear fashion, with an increase in frequency (Fig. 4 D). The present findings suggest that sarcomeric auto-oscillatory properties may operate physiologically upon relaxation by facilitating relaxation (lengthening) to adjacent sarcomeres (Stehle et al., 2006). However, care should be taken in the interpretation of the data; because the stiffness of the glass is higher than that of cardiac tissue, the sarcomere dynamics observed in the present study may reflect the properties of a cardiomyocyte attached to the glass surface rather than that under physiological situations (i.e., in the heart).

Here, it should be noted that although cell-SPOC occurs at partial activation (pCa 5.75 in the present study) and its waveform properties are similar to those obtained under electric field stimulation (compare with Fig. 4), cell-SPOC should be regarded as a useful experimental system that reveals important characteristics of sarcomere dynamics (e.g., shortening and lengthening properties, oscillation frequency, and the magnitude of contraction [Z-disc amplitude]) in living cardiomyocytes. Future studies are needed to conduct SL nanometry in the beating heart in vivo to investigate whether or not sarcomeric auto-oscillations indeed occur under physiological conditions at various developmental stages.

Recently, we constructed a mathematical model of SPOC (Ishiwata et al., 2011; Sato et al., 2011, 2013). In the model analysis, we demonstrated that an increase in the myosin attachment rate (α) results in an increase in amplitude and a decrease in frequency via an increase in shortening time. We therefore consider that a variance of regional $[Ca^{2+}]_i$ around myofilaments in neonatal myocytes (and thus a variance in α; see Ishiwata et al., 2011; Sato et al., 2011, 2013 for effects of Ca^{2+} on the myosin attachment rate), albeit by a small magnitude, modulates the properties of cell-SPOC. Consistent with this interpretation, at frequencies <1.5 Hz, the values of SL at peak shortening became <1.6 µm (i.e., shorter than the A-band length; Fig. 4 E), indicating that substantial actomyosin-based force was generated upon shortening. With an increase in frequency, maximal SL decreased and minimal SL increased, both in a linear

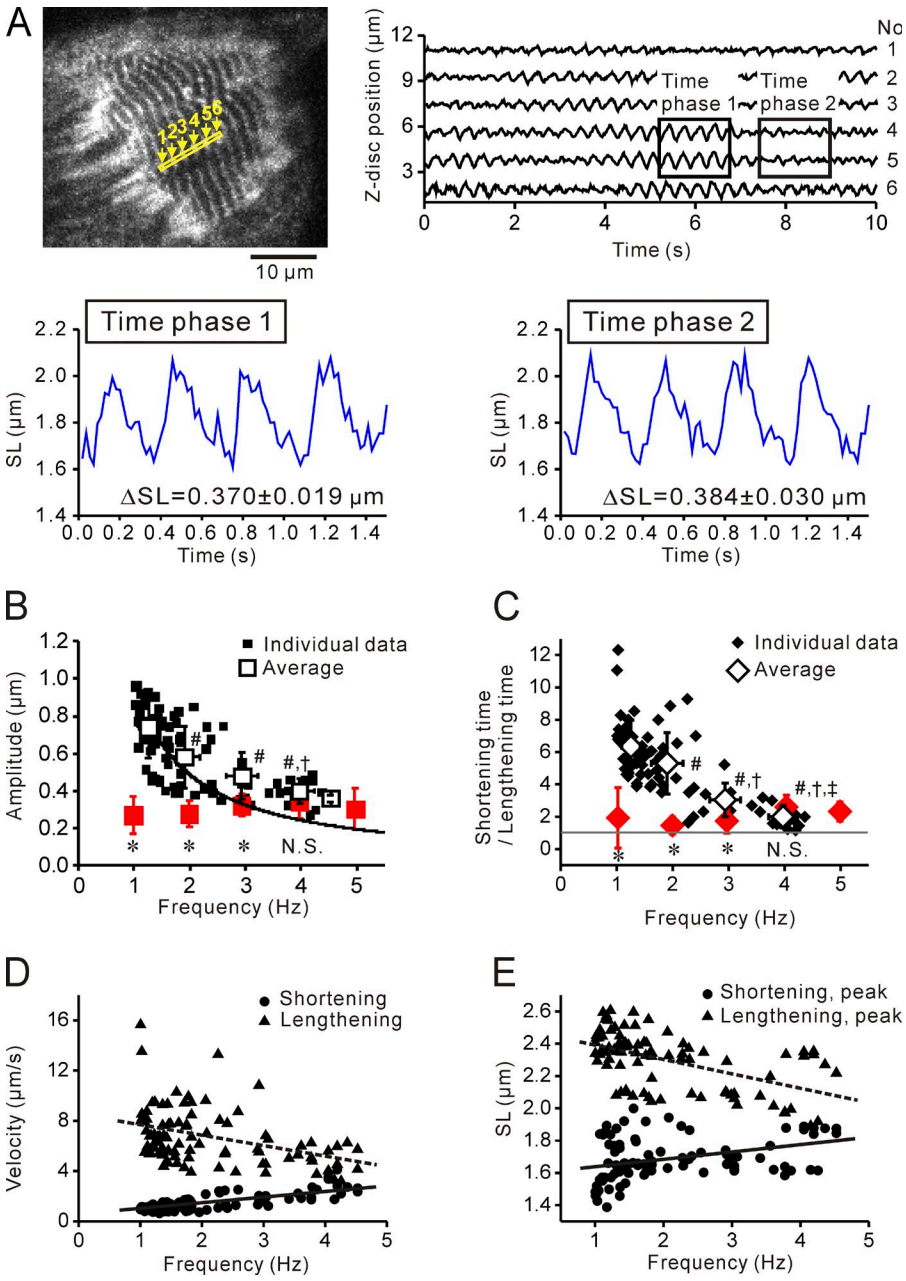

Figure 4. Cell-SPOC in neonatal cardiomyocytes. (A, top left) Epi-illumination image of an AcGFP-treated myocyte after ionomycin treatment in the presence of 200 µM ryanodine and 4 µM thapsigargin. The area in the yellow outlined rectangle was used for the SL analysis. (top right) Time course of changes in the positions of the Z discs, 1–6. Amplitude of the movement of Z disc 4 was 0.960 ± 0.023 and 0.385 ± 0.055 µm ($P < 0.05$) in time phases 1 and 2, respectively. Amplitude of the movement of Z disc 5 was 0.904 ± 0.041 and 0.461 ± 0.031 µm ($P < 0.05$) in time phases 1 and 2, respectively. (bottom) Waveform properties during cell-SPOC in time phases 1 and 2. Numbers in graphs indicate the mean values of the SL amplitude during cell-SPOC ($P > 0.05$). See Video 10. (B) Relationship of frequency versus amplitude in cell-SPOC. Individual data were fitted by a curve $Y = 0.974X^{-1}$ ($R = 0.618$; black line). The red squares were taken from Fig. 3 C (bottom). (C) Relationship of frequency versus the ratio of shortening time to lengthening time in cell-SPOC. The red diamonds were obtained from Fig. S9 (A and B). Gray line, shortening time/lengthening time = 1. (B and C) *, $P < 0.05$ compared with the values for cell-SPOC. #, $P < 0.05$; †, $P < 0.05$; ‡, $P < 0.05$ compared with 1, 2, and 3 Hz, respectively. (D) Relationship of frequency versus shortening (or lengthening) velocity in cell-SPOC. A significant linear relationship was obtained: $Y = 0.511X + 0.425$ ($R = 0.788$; $P < 0.0001$) for shortening (solid line) and $Y = -0.853X + 8.456$ ($R = 0.390$; $P < 0.0001$) for lengthening (dashed line). (E) Relationship of frequency versus maximal (or minimal) SL in cell-SPOC. Maximal and minimal SL values were obtained at peak lengthening (dashed line) and shortening (solid line), respectively. A significant linear relationship was obtained: $Y = 0.041X + 1.598$ ($R = 0.315$; $P < 0.002$) for minimal SL and $Y = -0.090X + 2.480$ ($R = 0.539$; $P < 0.0001$) for maximal SL. Note that minimal SL is <1.6 µm (1.58 µm; Luther et al., 2008); i.e., the length of the cardiac A band. Error bars indicate means ± SEM.

fashion, which is consistent with the notion that internal load along myofibrils is reduced as frequency increases (coupled with a decrease in α).

Finally, to explore whether SL nanometry can be used for the analysis of pharmacological actions of cardiac drugs, we investigated the effects of the actomyosin activator OM (Malik et al., 2011) on cell-SPOC. It has been reported that OM specifically targets and activates myocardial ATPase and improves energy utilization (Malik et al., 2011). In the present study, 0.6 µM OM did not affect amplitude of sarcomeric oscillations; rather, it significantly enhanced the Z-disc motion along myofibrils and shifted the relationship of SL amplitude versus Z-disc motion upward (Fig. 5 A and Video 12). The enhanced Z-disc amplitude likely results from an increase in actomyosin-based force along myofibrils and can be used as an index of contractility (as predicted by our SPOC model; Sato et al., 2011). OM increased (decreased) shortening time (shortening velocity; Fig. 5 B), but it did not significantly affect the lengthening properties

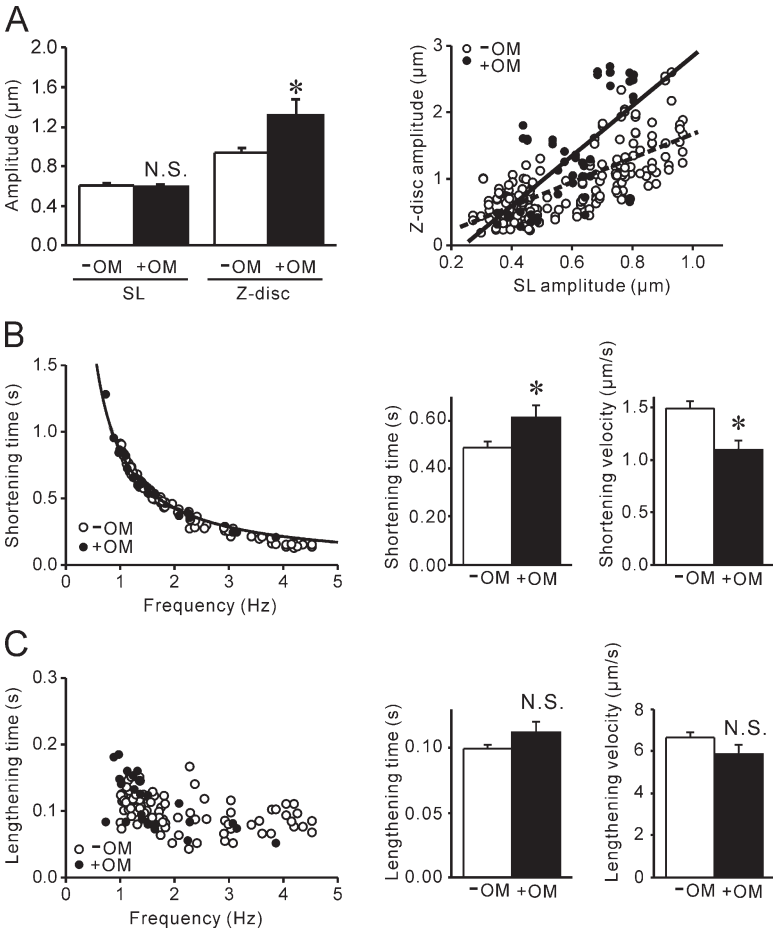

Figure 5. Effects of OM on cell-SPOC properties in neonatal cardiomyocytes. (A, left) Bar graph showing the values of the amplitude of SL oscillations and Z-disc oscillations in the absence and presence of OM. *, $P < 0.05$. (right) Relationship between SL amplitude versus Z-disc amplitude. Dashed line, –OM; solid line, +OM. A significant linear relationship was observed in the absence ($Y = 1.826X - 0.168$; $R = 0.726$; $P < 0.0001$) and presence ($Y = 3.827X - 0.944$; $R = 0.663$; $P < 0.0001$) of OM. (B, left) Relationship of cell-SPOC frequency versus shortening time. Open and closed circles indicate data in the absence (same as in Fig. S9 A) and presence of OM (taken from eight myocytes). Data were fitted by a curve $Y = 0.853X^{-1}$ ($R = 0.989$) in the presence of OM (compare with Fig. S9 A for the curve in the absence of OM). (right) Bar graphs showing mean values of shortening time or shortening velocity in the absence or presence of OM. *, $P < 0.05$. (C) Relationship of cell-SPOC frequency versus lengthening time. Open and closed circles indicate data in the absence (same as in Fig. S9 B) and presence of OM (taken from eight myocytes). Curve fitting was not performed because of the absence of a significant correlation. (right) Bar graphs showing mean values of lengthening time or lengthening velocity in the absence or presence of OM. *, $P < 0.05$. Error bars indicate means ± SEM.

(Fig. 5 C), thereby decreasing the cell-SPOC frequency (i.e., 1.63 ± 0.16 Hz on average from eight myocytes; $P < 0.05$ compared with the value obtained in the absence of OM, 2.08 ± 0.11 Hz). These experimental findings can be qualitatively explained by our SPOC model, which takes into account the "molecular friction" (i.e., the friction between actin and myosin; η [$\sim 1/\beta$, where β is the crossbridge detachment rate] in our SPOC model; Sato et al., 2011) in addition to α (myosin attachment rate). Table 1 summarizes the possible effects of OM on α and η and ensuing changes in cell-SPOC properties. If OM, as an actomyosin activator, increases α and decreases β, then η will be increased, resulting in a decrease in shortening velocity (and hence frequency), as found in the present study (Fig. 5 and Fig. S10). Our model likewise predicts that an increase in η decreases amplitude (Sato et al., 2011), and, accordingly, this effect will offset the increase in amplitude coupled with an increase in α (see Fig. 5 A for no significant effect of OM on cell-SPOC amplitude).

In conclusion, we developed a novel experimental system with cardiomyocytes allowing for nanoimaging of sarcomeric dynamic properties. This system is useful for analyzing cardiac excitation–contraction coupling at nanometer precision and for determining the changes in health and disease during development in future studies.

We thank Dr. Yuta Shimamoto for critical reading of the manuscript.

TABLE 1

Summary of cell-SPOC parameters used for the discussion on the experimental findings of OM

Parameter	Physiological meaning	+OM		
		Parameter change	Amplitude	Frequency
α	Crossbridge attachment rate	↑	↑	↓
η	Molecular frictional constant for crossbridge formation	↑	↓	↓

Our mathematical model (Sato et al., 2011) predicts that OM decreases frequency via an increase in α and an increase in η, but the compound hardly changes amplitude because the effect of an increase in α is offset by that of an increase in η (see Results and discussion). Amplitude, cell-SPOC amplitude; frequency, cell-SPOC frequency. Arrows, directions of change.

This work was supported in part by Grants-in-Aid for Scientific Research (B) (to N. Fukuda), Challenging Exploratory Research (to N. Fukuda and F. Kobirumaki-Shimozawa), Scientific Research on Innovative Areas (to N. Fukuda), and Specially Promoted Research and Scientific Research (S) (to S. Ishiwata) from the Ministry of Education, Culture, Sports, Science and Technology of Japan. This study was also supported in part by the Sasagawa Scientific Research Grant from the Japan Science Society (to S.A. Shintani).

The authors declare no competing financial interests.

Richard L. Moss served as editor.

Submitted: 10 October 2013
Accepted: 18 February 2014

REFERENCES

Allen, D.G., and J.C. Kentish. 1985. The cellular basis of the length-tension relation in cardiac muscle. *J. Mol. Cell. Cardiol.* 17:821–840. http://dx.doi.org/10.1016/S0022-2828(85)80097-3

Bers, D.M. 2002. Cardiac excitation-contraction coupling. *Nature.* 415:198–205. http://dx.doi.org/10.1038/415198a

Botcherby, E.J., A. Corbett, R.A. Burton, C.W. Smith, C. Bollensdorff, M.J. Booth, P. Kohl, T. Wilson, and G. Bub. 2013. Fast measurement of sarcomere length and cell orientation in Langendorff-perfused hearts using remote focusing microscopy. *Circ. Res.* 113:863–870. http://dx.doi.org/10.1161/CIRCRESAHA.113.301704

Boulesteix, T., E. Beaurepaire, M.P. Sauviat, and M.C. Schanne-Klein. 2004. Second-harmonic microscopy of unstained living cardiac myocytes: measurements of sarcomere length with 20-nm accuracy. *Opt. Lett.* 29:2031–2033. http://dx.doi.org/10.1364/OL.29.002031

Bub, G., P. Camelliti, C. Bollensdorff, D.J. Stuckey, G. Picton, R.A. Burton, K. Clarke, and P. Kohl. 2010. Measurement and analysis of sarcomere length in rat cardiomyocytes in situ and in vitro. *Am. J. Physiol. Heart Circ. Physiol.* 298:H1616–H1625. http://dx.doi.org/10.1152/ajpheart.00481.2009

Colella, M., F. Grisan, V. Robert, J.D. Turner, A.P. Thomas, and T. Pozzan. 2008. Ca^{2+} oscillation frequency decoding in cardiac cell hypertrophy: Role of calcineurin/NFAT as Ca^{2+} signal integrators. *Proc. Natl. Acad. Sci. USA.* 105:2859–2864. http://dx.doi.org/10.1073/pnas.0712316105

Dabiri, G.A., K.K. Turnacioglu, J.M. Sanger, and J.W. Sanger. 1997. Myofibrillogenesis visualized in living embryonic cardiomyocytes. *Proc. Natl. Acad. Sci. USA.* 94:9493–9498. http://dx.doi.org/10.1073/pnas.94.17.9493

Davidson, G.A., and R.J. Varhol. 1995. Kinetics of thapsigargin-Ca^{2+}-ATPase (sarcoplasmic reticulum) interaction reveals a two-step binding mechanism and picomolar inhibition. *J. Biol. Chem.* 270:11731–11734. http://dx.doi.org/10.1074/jbc.270.20.11731

Drago, I., D. De Stefani, R. Rizzuto, and T. Pozzan. 2012. Mitochondrial Ca^{2+} uptake contributes to buffering cytoplasmic Ca^{2+} peaks in cardiomyocytes. *Proc. Natl. Acad. Sci. USA.* 109:12986–12991. http://dx.doi.org/10.1073/pnas.1210718109

Fukuda, N., D. Sasaki, S. Ishiwata, and S. Kurihara. 2001. Length Dependence of Tension Generation in Rat Skinned Cardiac Muscle: Role of Titin in the Frank-Starling Mechanism of the Heart. *Circulation.* 104:1639–1645. http://dx.doi.org/10.1161/hc3901.095898

Gonda, K., T.M. Watanabe, N. Ohuchi, and H. Higuchi. 2010. In vivo nano-imaging of membrane dynamics in metastatic tumor cells using quantum dots. *J. Biol. Chem.* 285:2750–2757. http://dx.doi.org/10.1074/jbc.M109.075374

Gregorio, C.C., H. Granzier, H. Sorimachi, and S. Labeit. 1999. Muscle assembly: a titanic achievement? *Curr. Opin. Cell Biol.* 11:18–25. http://dx.doi.org/10.1016/S0955-0674(99)80003-9

Hanft, L.M., F.S. Korte, and K.S. McDonald. 2008. Cardiac function and modulation of sarcomeric function by length. *Cardiovasc. Res.* 77:627–636. http://dx.doi.org/10.1093/cvr/cvm099

Hersch, N., B. Wolters, G. Dreissen, R. Springer, N. Kirchgeßner, R. Merkel, and B. Hoffmann. 2013. The constant beat: cardiomyocytes adapt their forces by equal contraction upon environmental stiffening. *Biol. Open.* 2:351–361. http://dx.doi.org/10.1242/bio.20133830

Inoue, T., F. Kobirumaki-Shimozawa, T. Kagemoto, T. Fujii, T. Terui, Y. Kusakari, K. Hongo, S. Morimoto, I. Ohtsuki, K. Hashimoto, and N. Fukuda. 2013. Depressed Frank-Starling mechanism in the left ventricular muscle of the knock-in mouse model of dilated cardiomyopathy with troponin T deletion mutation ΔK210. *J. Mol. Cell. Cardiol.* 63:69–78. http://dx.doi.org/10.1016/j.yjmcc.2013.07.001

Ishiwata, S., Y. Shimamoto, and N. Fukuda. 2011. Contractile system of muscle as an auto-oscillator. *Prog. Biophys. Mol. Biol.* 105:187–198. http://dx.doi.org/10.1016/j.pbiomolbio.2010.11.009

Jacot, J.G., A.D. McCulloch, and J.H. Omens. 2008. Substrate stiffness affects the functional maturation of neonatal rat ventricular myocytes. *Biophys. J.* 95:3479–3487. http://dx.doi.org/10.1529/biophysj.107.124545

Jacot, J.G., H. Kita-Matsuo, K.A. Wei, H.S. Chen, J.H. Omens, M. Mercola, and A.D. McCulloch. 2010. Cardiac myocyte force development during differentiation and maturation. *Ann. N.Y. Acad. Sci.* 1188:121–127. http://dx.doi.org/10.1111/j.1749-6632.2009.05091.x

Katz, A.M. 2002. Ernest Henry Starling, his predecessors, and the "Law of the Heart". *Circulation.* 106:2986–2992. http://dx.doi.org/10.1161/01.CIR.0000040594.96123.55

Kauffman, R.F., R.W. Taylor, and D.R. Pfeiffer. 1980. Cation transport and specificity of ionomycin. Comparison with ionophore A23187 in rat liver mitochondria. *J. Biol. Chem.* 255:2735–2739.

Kaya, M., and H. Higuchi. 2010. Nonlinear elasticity and an 8-nm working stroke of single myosin molecules in myofilaments. *Science.* 329:686–689. http://dx.doi.org/10.1126/science.1191484

King, N.M., M. Methawasin, J. Nedrud, N. Harrell, C.S. Chung, M. Helmes, and H. Granzier. 2011. Mouse intact cardiac myocyte mechanics: cross-bridge and titin-based stress in unactivated cells. *J. Gen. Physiol.* 137:81–91. http://dx.doi.org/10.1085/jgp.201010499

Kojima, K., H. Moriguchi, A. Hattori, T. Kaneko, and K. Yasuda. 2003. Two-dimensional network formation of cardiac myocytes in agar microculture chip with 1480 nm infrared laser photo-thermal etching. *Lab Chip.* 3:292–296. http://dx.doi.org/10.1039/b304652d

Komori, T., S. Nishikawa, T. Ariga, A.H. Iwane, and T. Yanagida. 2009. Simultaneous measurement of nucleotide occupancy and mechanical displacement in myosin-V, a processive molecular motor. *Biophys. J.* 96:L4–L6. http://dx.doi.org/10.1016/j.bpj.2008.09.031

Lahmers, S., Y. Wu, D.R. Call, S. Labeit, and H. Granzier. 2004. Developmental control of titin isoform expression and passive stiffness in fetal and neonatal myocardium. *Circ. Res.* 94:505–513. http://dx.doi.org/10.1161/01.RES.0000115522.52554.86

Llewellyn, M.E., R.P. Barretto, S.L. Delp, and M.J. Schnitzer. 2008. Minimally invasive high-speed imaging of sarcomere contractile dynamics in mice and humans. *Nature.* 454:784–788.

Luther, P.K., P.M. Bennett, C. Knupp, R. Craig, R. Padrón, S.P. Harris, J. Patel, and R.L. Moss. 2008. Understanding the organisation and role of myosin binding protein C in normal striated muscle by comparison with MyBP-C knockout cardiac muscle. *J. Mol. Biol.* 384:60–72. http://dx.doi.org/10.1016/j.jmb.2008.09.013

Malik, F.I., J.J. Hartman, K.A. Elias, B.P. Morgan, H. Rodriguez, K. Brejc, R.L. Anderson, S.H. Sueoka, K.H. Lee, J.T. Finer, et al. 2011. Cardiac myosin activation: a potential therapeutic approach for systolic heart failure. *Science.* 331:1439–1443. http://dx.doi.org/10.1126/science.1200113

Morgan, A.J., and R. Jacob. 1994. Ionomycin enhances Ca^{2+} influx by stimulating store-regulated cation entry and not by a direct action at the plasma membrane. *Biochem. J.* 300:665–672.

Opitz, C.A., M.C. Leake, I. Makarenko, V. Benes, and W.A. Linke. 2004. Developmentally regulated switching of titin size alters myofibrillar stiffness in the perinatal heart. *Circ. Res.* 94:967–975. http://dx.doi.org/10.1161/01.RES.0000124301.48193.E1

Oyama, K., A. Mizuno, S.A. Shintani, H. Itoh, T. Serizawa, N. Fukuda, M. Suzuki, and S. Ishiwata. 2012. Microscopic heat pulses induce contraction of cardiomyocytes without calcium transients. *Biochem. Biophys. Res. Commun.* 417:607–612. http://dx.doi.org/10.1016/j.bbrc.2011.12.015

Peterson, P., M. Kalda, and M. Vendelin. 2013. Real-time determination of sarcomere length of a single cardiomyocyte during contraction. *Am. J. Physiol. Cell Physiol.* 304:C519–C531. http://dx.doi.org/10.1152/ajpcell.00032.2012

Plotnikov, S.V., A.C. Millard, P.J. Campagnola, and W.A. Mohler. 2006. Characterization of the myosin-based source for second-harmonic generation from muscle sarcomeres. *Biophys. J.* 90:693–703. http://dx.doi.org/10.1529/biophysj.105.071555

Rodriguez, A.G., S.J. Han, M. Regnier, and N.J. Sniadecki. 2011. Substrate stiffness increases twitch power of neonatal cardiomyocytes in correlation with changes in myofibril structure and intracellular calcium. *Biophys. J.* 101:2455–2464. http://dx.doi.org/10.1016/j.bpj.2011.09.057

Sasaki, D., N. Fukuda, and S. Ishiwata. 2006. Myocardial sarcomeres spontaneously oscillate with the period of heartbeat under physiological conditions. *Biochem. Biophys. Res. Commun.* 343:1146–1152. http://dx.doi.org/10.1016/j.bbrc.2006.03.070

Sato, K., M. Ohtaki, Y. Shimamoto, and S. Ishiwata. 2011. A theory on auto-oscillation and contraction in striated muscle. *Prog. Biophys. Mol. Biol.* 105:199–207. http://dx.doi.org/10.1016/j.pbiomolbio.2010.12.003

Sato, K., Y. Kuramoto, M. Ohtaki, Y. Shimamoto, and S. Ishiwata. 2013. Locally and Globally Coupled Oscillators in Muscle. *Phys. Rev. Lett.*111:108104–108109.http://dx.doi.org/10.1103/PhysRevLett.111.108104

Serizawa, T., T. Terui, T. Kagemoto, A. Mizuno, T. Shimozawa, F. Kobirumaki, S. Ishiwata, S. Kurihara, and N. Fukuda. 2011. Real-time measurement of the length of a single sarcomere in rat ventricular myocytes: a novel analysis with quantum dots. *Am. J. Physiol. Cell Physiol.* 301:C1116–C1127. http://dx.doi.org/10.1152/ajpcell.00161.2011

Smotherman, W.P., S.R. Robinson, A.E. Ronca, J.R. Alberts, and P.G. Hepper. 1991. Heart rate response of the rat fetus and neonate to a chemosensory stimulus. *Physiol. Behav.* 50:47–52. http://dx.doi.org/10.1016/0031-9384(91)90496-B

Stehle, R., J. Solzin, B. Iorga, D. Gomez, N. Blaudeck, and G. Pfitzer. 2006. Mechanical properties of sarcomeres during cardiac myofibrillar relaxation: stretch-induced cross-bridge detachment contributes to early diastolic filling. *J. Muscle Res. Cell Motil.* 27:423–434. http://dx.doi.org/10.1007/s10974-006-9072-7

Sutko, J.L., J.A. Airey, W. Welch, and L. Ruest. 1997. The pharmacology of ryanodine and related compounds. *Pharmacol. Rev.* 49:53–98.

Tada, H., H. Higuchi, T.M. Wanatabe, and N. Ohuchi. 2007. In vivo real-time tracking of single quantum dots conjugated with monoclonal anti-HER2 antibody in tumors of mice. *Cancer Res.* 67:1138–1144. http://dx.doi.org/10.1158/0008-5472.CAN-06-1185

Treiman, M., C. Caspersen, and S.B. Christensen. 1998. A tool coming of age: thapsigargin as an inhibitor of sarco-endoplasmic reticulum Ca^{2+}-ATPases. *Trends Pharmacol. Sci.* 19:131–135. http://dx.doi.org/10.1016/S0165-6147(98)01184-5

Udaka, J., S. Ohmori, T. Terui, I. Ohtsuki, S. Ishiwata, S. Kurihara, and N. Fukuda. 2008. Disuse-induced preferential loss of the giant protein titin depresses muscle performance via abnormal sarcomeric organization. *J. Gen. Physiol.* 131:33–41. http://dx.doi.org/10.1085/jgp.200709888

Uemura, S., H. Higuchi, A.O. Olivares, E.M. De La Cruz, and S. Ishiwata. 2004. Mechanochemical coupling of two substeps in a single myosin V motor. *Nat. Struct. Mol. Biol.* 11:877–883. http://dx.doi.org/10.1038/nsmb806

Watanabe, T.M., F. Fujii, T. Jin, E. Umemoto, M. Miyasaka, H. Fujita, and T. Yanagida. 2013. Four-dimensional spatial nanometry of single particles in living cells using polarized quantum rods. *Biophys. J.* 105:555–564. http://dx.doi.org/10.1016/j.bpj.2013.07.001

Werdich, A.A., E.A. Lima, I. Dzhura, M.V. Singh, J. Li, M.E. Anderson, and F.J. Baudenbacher. 2008. Differential effects of phospholamban and Ca^{2+}/calmodulin-dependent kinase II on $[Ca^{2+}]_i$ transients in cardiac myocytes at physiological stimulation frequencies. *Am. J. Physiol. Heart Circ. Physiol.* 294:H2352–H2362. http://dx.doi.org/10.1152/ajpheart.01398.2006

Yoo, J., T. Kambara, K. Gonda, and H. Higuchi. 2008. Intracellular imaging of targeted proteins labeled with quantum dots. *Exp. Cell Res.* 314:3563–3569. http://dx.doi.org/10.1016/j.yexcr.2008.09.014